# Prediction of hydraulically transmissive fractures using geological and geophysical attributes: a case history from the mid Jhuoshuei River basin, Taiwan

**Po-Yi Chou · Hung-Chieh Lo · Shih-Meng Hsu · Yen-Tsu Lin · Chi-Chao Huang**

**Abstract** The feasibility of using geological and geophysical well-log and borehole-televiewer data for the identification of hydraulically transmissive fractures is evaluated. Twenty-nine boreholes were drilled to a depth of 100m in the middle-stream basin of Jhuoshuei River, Taiwan. Four criteria that assist in indicating the potential presence of permeable zones are proposed, including: lower gamma-ray response compared with the average response, divergence of the short normal-resistivity log relative to that of the long one, longer sonic travel time, and the appearance of discernible openings detected with the televiewer. With these, the transmissivities at the predetermined depths were estimated and verified by an in-situ hydraulic test. The statistical results indicate that, particularly in the mountainous area where a complex folded structure with a succession of synclines and anticlines is shown, the interpretation of lithologic conditions is not necessary to identify the presence of a relatively higher-permeability zone. Comparatively, the estimates of porosity and fracture aperture are the necessary premises to the prediction of hydraulically transmissive fractures. A joint consideration of all four criteria is found, allowing a less biased evaluation of the fracture transmissivity.

**Keywords** Fractured rocks · Groundwater hydraulics · Hydraulic testing · Geophysical methods · Taiwan

Received: 15 May 2011 / Accepted: 15 April 2012



P.-Y. Chou (✉) · H.-C. Lo · S.-M. Hsu
Geotechnical Engineering Research Center,
Sinotech Engineering Consultants, Inc.,
B1 No.7 Lane 26, Yet-sen Road, 110 Taipei, Taiwan
e-mail: poyi.chou@sinotech.org.tw
Tel.: +886-2-27580568
Fax: +886-2-27290237

H.-C. Lo
e-mail: jaylo@sinotech.org.tw

S.-M. Hsu
e-mail: shihmeng@sinotech.org.tw

Y.-T. Lin · C.-C. Huang
Central Geological Survey, MOEA, P.O. BOX 968, 235 Taipei, Taiwan

Y.-C. Lin
e-mail: ytlin@moeacgs.gov.tw

C.-C. Huang
e-mail: hjj@moeacgs.gov.tw

## Introduction

Adequate interpretation of the hydrogeological characteristics of mountainous regions is crucial. The rising need for sufficient potable water urges more understanding about the potential yield of aquifers. In mountainous areas, where stratified materials are commonly present, the movement of groundwater is either controlled by the fracture continua, or the intergranular pore spaces, or by both. The inherent physical properties of strata and the ambient tectonic stresses are deemed to play a pivotal role in determining the occurrence of preferential flow paths. The ambient tectonic stresses, as indicated by Lee et al. (1997), are the additional stresses deviated from lithostatic stress. With a combination of boundary forces and surface dynamic loads (Kaus et al. 2009), the change in tectonic stresses is capable of causing pore-fluid pressure perturbations (Chia et al. 2001), as well as modifying the porosity in natural rocks. Besides, the anisotropy of the hydraulic conductivity of the aquifer is found to be closely related to the accumulation of tectonic stress (Talbot and Sirat 2001; Bense et al. 2003; Henriksen 2006). Large uncertainties in model output are however presented owing to limited knowledge on the representative conductivities of the subsurface environment (Winter et al. 2003; Zhang et al. 2007). Consequently, prior to evaluating whether a stratum is capable of yielding or storing a sufficient amount of groundwater by means of any sophisticated numerical models, it is concurred that only by performing downhole geophysical investigation could


DOI 10.1007/s10040-012-0861-3

Published online: 12 May 2012

more in-depth insights be gained. One of the fundamental objectives is to determine the distribution of transmissivity ($T$) within stratified aquifers.

The flow of groundwater through fractures and rock matrix is governed by two mechanisms: the connectivity of the discontinuities and the vector gradient of hydraulic heads in the field. Philip et al. (2005) deduced that the bulk permeability of a fracture network can be 2–10 times higher than that of the matrix. Studies have also indicated that the estimates of fracture permeability in situ can be on scales larger than that from laboratory experiments (McKay et al. 1993; Doan et al. 2006), since core samples from the rock matrix are most commonly used and the actual permeability of the formation is prone to be underestimated (van der Kamp 2001). On the basis of their study of a hard-rock aquifer in India, Maréchal et al. (2004) pointed out that the conductive fractures contribute almost equivalently to the bulk horizontal conductivity of the aquifer. The occurrences of open fractures are thus regarded as the most dominated water-bearing pathway in the mountainous area. The identification of hydraulically transmissive fractures from the actual fracture network geometry is certainly crucial, but often difficult.

As pointed out by Marine (1980) and Niemi et al. (2000), possibly only a portion of perceptible open fractures within a stratum are truly hydrologically activated. The sealed-fractures that filled with minerals or clay deposit are always weak in water transmitting capacity. The identification of specific hydraulically transmissive fractures as distinct from other similar but non-productive ones is presenting challenges. The increase of topographic slope, as commonly occurring in the mountainous areas, would create fractures with varied orientations and thus lead to significantly large anisotropy in the spatial distribution of hydraulic conductivity (Zhang et al. 2007). Dynamics of groundwater flow through the fracture continua may not be simply predicted from the basic flow regimes or the conventional well-flow equations (Matthäi 2003; Maréchal et al. 2004). Presumably, as indicated by Barton et al. (1995), the reason for some fractures being more hydraulically conductive than others is poorly understood and calls for further research.

Even though the establishment of interrelations between fracture attributes and hydraulic properties has frequently been assessed (Guimerà and Carrera, 1997; Morin et al. 1997, 2000; Hamm et al. 2007), most of the correlations are however empirical and site specific. A combination of composite well logs and in-hole tracer tests could provide more than sufficient insight into the complex geometries, but it might also lead to non-uniqueness of parameters in providing acceptable estimations (Becker and Shapiro, 2000). As concluded in the review of the National Research Council (1996), the inference of fracture parameters by different borehole or geophysical logs still retains significant uncertainty with respect to fluid flow. Great care is thus required, especially when working with limited cost and time, to develop a set of systematic and concise criteria for quickly identifying the presence of hydraulically transmissive fractures. This concern motivates the current study.

A large-scale hydrogeological investigation project was carried out in 2010, with support from the Central Geological Survey of Taiwan, which aimed at exploring in detail the hydraulic properties of bedrock aquifers in the mid-Taiwan mountainous area. The purpose of this paper is to outline the major findings, with particular emphasis on the feasibility of using geological and geophysical well-log and borehole-televiewer data for the identification of hydraulically transmissive fractures.

## Geological description of the study area

The study area is located in the western foothills of Taiwan at the latitude and longitude of 23° 40' N and 120° 45' E, respectively. It covers the Douliu Hill and the midstream of the Jhuoshuei River with an area of 1,577 $km^2$. The elevation lies between 21 and 3,931 meters above sea level (m a.s.l.). Owing to the collision of tectonic plates (Mouthereau and Lacombe 2006), a series of westward fold-and-thrust belts can be observed in the study area. The geological formation in this study area can be roughly separated from east to west into four regions simply by the orientation of faults. As shown in Fig. 1, the region A at the most eastern side ranges in age from Eocene to Miocene, where the predominant lithology is a massive, thick slate rock but some metasandstones and metasiltstones do occur. Bordered by the Dili fault, the region B extends from Eocene to early Oligocene, where the upper part is dominated by hard shale stone and the lower part is coarse quartz sandstone. The region C, bounded by the Shuilikeng, Chelungpu and Tachienshan faults, is underlain by Miocene to Pleistocene sedimentary rocks. A distinct pattern of lithological distribution can be found and closely related to the influence of folding, faulting and metamorphism. In region C, beneath the near-surface regolith layer, the bedrock is mainly composed of hard shale and coarse quartz sandstone. The region D at the most western side is mainly consisted of semi-consolidated alluvium and relatively young deposits from late Pliocene to Pleistocene.

Topographic slopes in region A, B and C are from 58 to 173 %, while relatively gentle topographic slopes (< 58 %) are formed in region D. Most of the study area is covered by a regolith layer, which is the unconsolidated weathering zone consisting of soil, backfills, alluvium, colluvium, and saprolite. The apparent thickness of regolith layer in region A, B and C is approximately 18 m, except at the site of borehole B11 where more than 50 m of regolith layer was measured, while in region D a wide variation of the regolith thickness is observed. It was found that the unconsolidated sediments at the site of borehole BH03, BH14, BH28 and BH29 are much greater than 100 m, which accounts for the top of the bedrock being far deeper than expected.


DOI 10.1007/s10040-012-0861-3

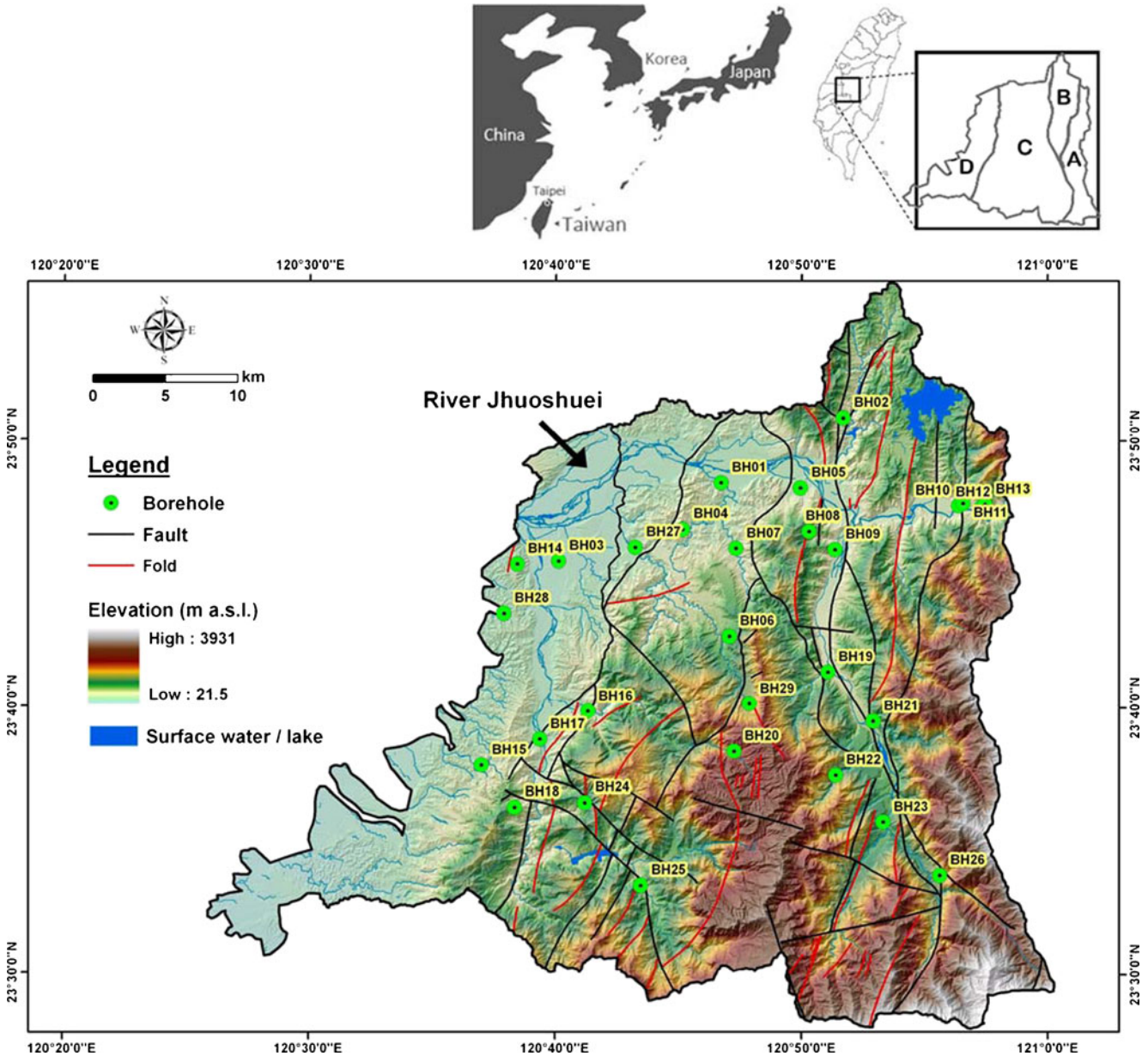


**Fig. 1** Elevation profile of mid-Jhuoshuei River basin

## Methodology

A total of 29 vertical boreholes (see Table 1) were drilled to at least 100 m (328 ft) below land surface. For performing the packer testing, the combination of mechanical and pneumatic drilling rigs with drilling coring size of 6.3 cm (HQ bits) was adopted. As can be seen in Fig. 1, the region C covers the largest portion of the study area, accordingly, more than half of the boreholes were drilled in this region. Rock samples were recovered and prepared for an initial on-site lithostratigraphic identification carried out by licensed geologists, as well as various laboratory analyses afterward. According to the driller's log and the geologists' report, a general characterization of fractures within the rock mass was presented. Four predominant bedrock types are distinguished in this study area: quartzite, slate, sandstone and shale. As the flowchart of investigation shows (in Fig. 2), in each borehole, prior to performing the downhole hydraulic packer test, a series of borehole loggings were conducted in situ to identify all probable conductive pathways.

### *Geophysical logging*

The spatial variability of fine-scale geophysical parameters was documented by the electric log (ELOG) and the full waveform sonic log (SLOG; from Robertson Geologging Ltd. UK). Both types of sonde have long been widely used in the field of geosciences to provide a variety of lithologic information; a comprehensive overview has


DOI 10.1007/s10040-012-0861-3

**Table 1** Description of boreholes

| Topographic region | Borehole | Geometric height (m a.s.l.) | Regolith thickness (m) | Groundwater level[a] (m a.s.l.) |
|---|---|---|---|---|
| A | BH11 | 391 | 50.2 | 377 |
| | BH12 | 472 | 1.6 | 395 |
| | BH13 | 468 | 0.6 | 382 |
| B | BH02 | 431 | 12.7 | 427 |
| | BH10 | 357 | 4.4 | 348 |
| | BH21 | 638 | 14.5 | 602 |
| C | BH04 | 409 | 20.0 | 405 |
| | BH05 | 295 | 41.8 | 284 |
| | BH06 | 764 | 9.4 | 754 |
| | BH08 | 633 | 19.5 | 629 |
| | BH09 | 403 | 41.6 | 387 |
| | BH16 | 280 | 17.8 | 266 |
| | BH17 | 227 | 5.4 | 223 |
| | BH18 | 631 | 20.0 | 608 |
| | BH19 | 476 | 20.0 | 456 |
| | BH20 | 1,658 | 14.4 | 1605 |
| | BH22 | 943 | 14.7 | 930 |
| | BH24 | 756 | 6.0 | 743 |
| | BH25 | 712 | 17.5 | 697 |
| | BH26 | 1,172 | 8.0 | 1,165 |
| | BH27 | 191 | 5.6 | 185 |
| | BH29 | 1,201 | >100 | 1,183 |
| D | BH01 | 316 | 8.3 | 314 |
| | BH03 | 142 | >100 | 138 |
| | BH07 | 345 | 9.5 | 340 |
| | BH14 | 341 | >100 | 261 |
| | BH15 | 312 | 1.7 | 284 |
| | BH23 | 749 | 11.7 | 740 |
| | BH28 | 188 | >100 | 179 |

[a] Groundwater level data were collected in October 2010

been provided in the study of Timur and Toksöz (1985), Keys (1990), and Lau (1998). In this present research, ELOG was used to measure the spontaneous potential (SP), electrical resistivity (ER) and natural gamma radiation (GR), while SLOG was applied to detect the sonic travel-time ($\Delta t$) at a specific depth within the borehole.

- The SP log measures the electrochemical potential difference between the mud filtrate and formation water salinities (Keys, 1990); the salinity of fluid is inversely proportional to its resistivity. It is recorded directly in millivolts (mV), and the deflection of signal with depth tends to be relatively larger in the case of a permeable stratum (e.g. sandstone) than in an impermeable one (e.g., shale). Chow et al. (2005) indicated that the deflection on SP reading is controlled locally by permeability. However, the application of the SP log in the mountainous area is limited since it was found that conductive borehole fluids were required during the logging process (usually the salinity of formation water in the mountainous area is far lower that these fluids). So it is considered that the SP log may offer a rapid and broad identification of the range of permeable formations, but not their hydrolithological properties.
- The ER log measures the resistance of formation fluid to the induced electrical current, which is closely related to the effective porosity of aquifer materials, amount of macro pores, grain size, and water saturation (Keys, 1990; Helm-Clark et al. 2004; Hsieh et al. 2005). The effective porosity, as defined by Keys (1990) and Hall et al. (1991), is the total volume of interconnected pore spaces in the rock that is capable of contributing to groundwater flow. The magnitude of effective porosity equals the magnitude of total porosity, excluding, if any, the clay-bound fraction. The ER log can be used to record the single-point resistance in ohms (Ω) and the normal resistivity in ohm-meters (Ω-m or ohm-m). The prospecting range is governed by the electrode spacing, which is typically set to be either 16 (short) or 64 (long) inches (1 inch≈ 2.54 cm). In general, the short-normal log provides higher resolution in delineating the resistance for specific focal rocks or fracture zones. Helm-Clark et al. (2004) pointed out that the permeable zones could possibly be identified by comparing the short normal-resistivity log relatively to the long one. Ellis and Ross (2007) deemed that generally both signals tend to coincide with each other in the sandstone-dominant formations, however, a deflection of short-normal log relative to the long one could be attributed to the intervention of drilling mud as a result of the higher stratum permeability.

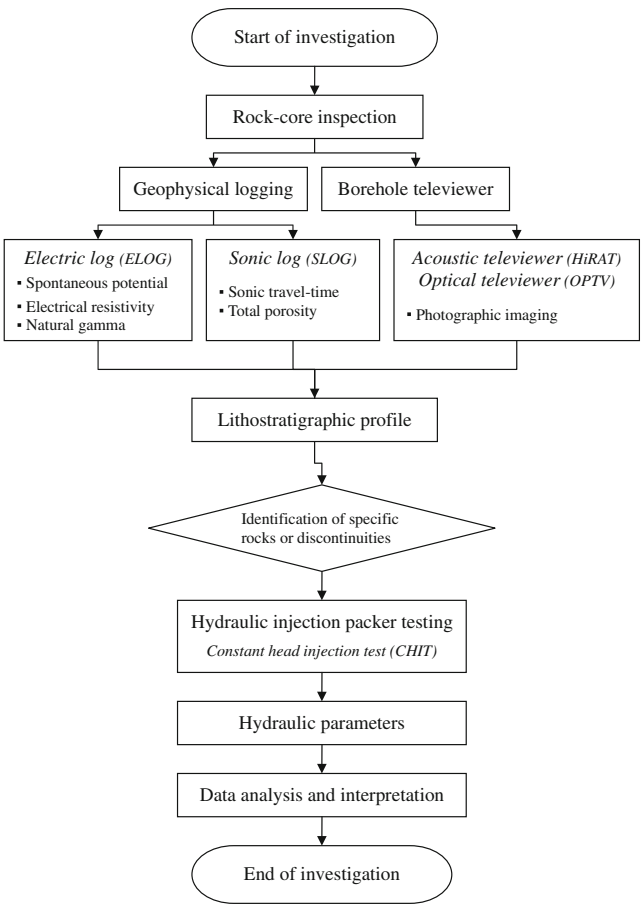


**Fig. 2** Flow-chart of investigation


DOI 10.1007/s10040-012-0861-3

The same speculation was also given by Chapellier (1992) and Hsieh et al. (2005).

– The GR log quantifies the natural gamma radiation emanating from the rock surrounding the borehole. The gamma-ray signal in the formation is recorded by the detector (scintillation counter) and then converted into an electrical pulse by the photomultiplier. It is recorded in units of counts-per-second (cps) and primarily in accordance with the clay content. In igneous and metamorphic rocks, the response of the gamma-ray log corresponds to the felsic mineral content (Lau 1998). In sedimentary rocks, relatively high gamma radiation is present in the fine-grained deposits such as the shaly rock, which potentially contains significant amounts of radioactive elements. On the other hand, a low gamma-ray response indicates the presence of coarse-grained sandstone.
– The SLOG provides insight into the acoustic velocity of compressional waves in borehole fluid and surrounding rock, which is a function of lithological porosity. The sonic travel time ($\Delta t$), from the transmitter via the adjacent rock to the receiver, is correlated with the rock strength, elastic properties of formations, and the rock/matrix density. Typically, wave propagation in the formation containing openings or cavities takes substantially longer time. Correspondingly, the velocity-depth profile of consolidated igneous or metamorphic rock is relatively faster in comparison with that of unconsolidated rock. It therefore provides crucial evidence in identifying the integrity of rock mass along the borehole. In addition, the calculation in this study was made using ultrasonic waves with high frequency, near 500 kHz, which generates a wavelength of 0.01 m. The probe is equipped with three receivers at different distances away from the transmitter, which allows the suspect sonic logs to be filtered out as a precaution.

By using acoustic-velocity logging, as indicated by Wyllie et al. (1956), aquifer porosity can be determined based on the time-average equation as showing below:

$$\Delta t = \frac{1}{V_L} = \frac{\phi_s}{V_f} + \frac{1-\phi_s}{V_m} \quad \text{(Eq.1)}$$

where $\phi_s$ represents the sonic derived total porosity [$L^3$/$L^3$], which includes all of the interstices and pore space of the rock matrix; $V_L$ is the transit velocity of "sound" through a particular rock type, or formation, determined from the sonic log [L/T]; $V_f$ represents the velocity in the borehole fluid [L/T], which is about 1,524 m/sec in fresh water; $V_m$ represents the velocity of sound propagating in the rock matrix [L/T]. For the typical range of transit velocities for some common rocks, refer to Keys (1990). For the concerns of cycle-skipping, which is actually a hint indicating the presence of fractures in the hard rock formation (Keys 1990), cross comparison of driller's-logs and core logs was carried out during and after the field work, so that some unrealistic values such as extremely high travel time in the unconsolidated formation, were not taken into account in the final analysis. In the current study, the dynamic modulus of elasticity ($E_D$) was also determined, which is done by an independent laboratory, to ensure a more precise value for $V_m$ was obtained.

## Borehole televiewer

The application of borehole televiewers in fracture identification also has long been adopted (see earlier studies: Keys 1990; Williams and Johnson, 2004; Morin 2005; Hubbard et al. 2008). Borehole televiewing was performed to provide a visual indication of the formation and to un-wrap the oriented circular borehole-wall images, whereby not only the findings in the geologists' report can be confirmed, but the dip-azimuth, aperture, and infilling material can also be quantified by further mapping efforts. Within the potential zone of interest, the geological formation may consist of either more than one set of open-fractures, a broad zone of highly fractured rock mass, multi fine hairline-cracks with aperture less than 1 mm, or a combination of afore-mentioned attributes.

Two types of televiewer were adopted in this project to identify the appearance of fracture zones: the high resolution acoustic televiewer (HiRAT) and the optical televiewer (OPTV) (from Robertson Geologging Ltd. UK). The principle of the HiRAT probe is based on analyzing the travel-times and amplitudes of reflected acoustic wave from the borehole-wall and converting the signal into photographic images. For this reason, the HiRAT log has to be performed in a water-filled or mud-filled borehole only. Alternatively, the OPTV can be applied in both air and clean-water filled boreholes. By importing borehole images into the software package RGLDIP (version 6), each individual fracture aperture can be calculated.

## Interpretation of geophysical log and borehole televiewer data

Taking borehole BH25 as an example, the result of in-situ geophysical loggings and televiewer imaging is illustrated in Fig. 3. The accessible geophysical logging profile was displayed from 15 to 100 m depth; the measured groundwater level was 15.4 m below land surface, and the borehole was cased to a depth of 15 m due to the appearance of a regolith layer. The procedures for identifying probable conductive fracture zones were the following:

– Electric log: the spontaneous potential log with depth covers a range from 75 to 110 mV. A gradual rightward deflection is shown, which indicates a decreasing tendency of grain size towards the base (Chow et al. 2005). The gamma radiation log with depth varies in a range between 60 and 160 cps. As can be seen, seven sections with a lower gamma-ray response, and, simultaneously, pronounced oscillation or spike amplitude in the short normal-resistivity log relatively to the


DOI 10.1007/s10040-012-0861-3

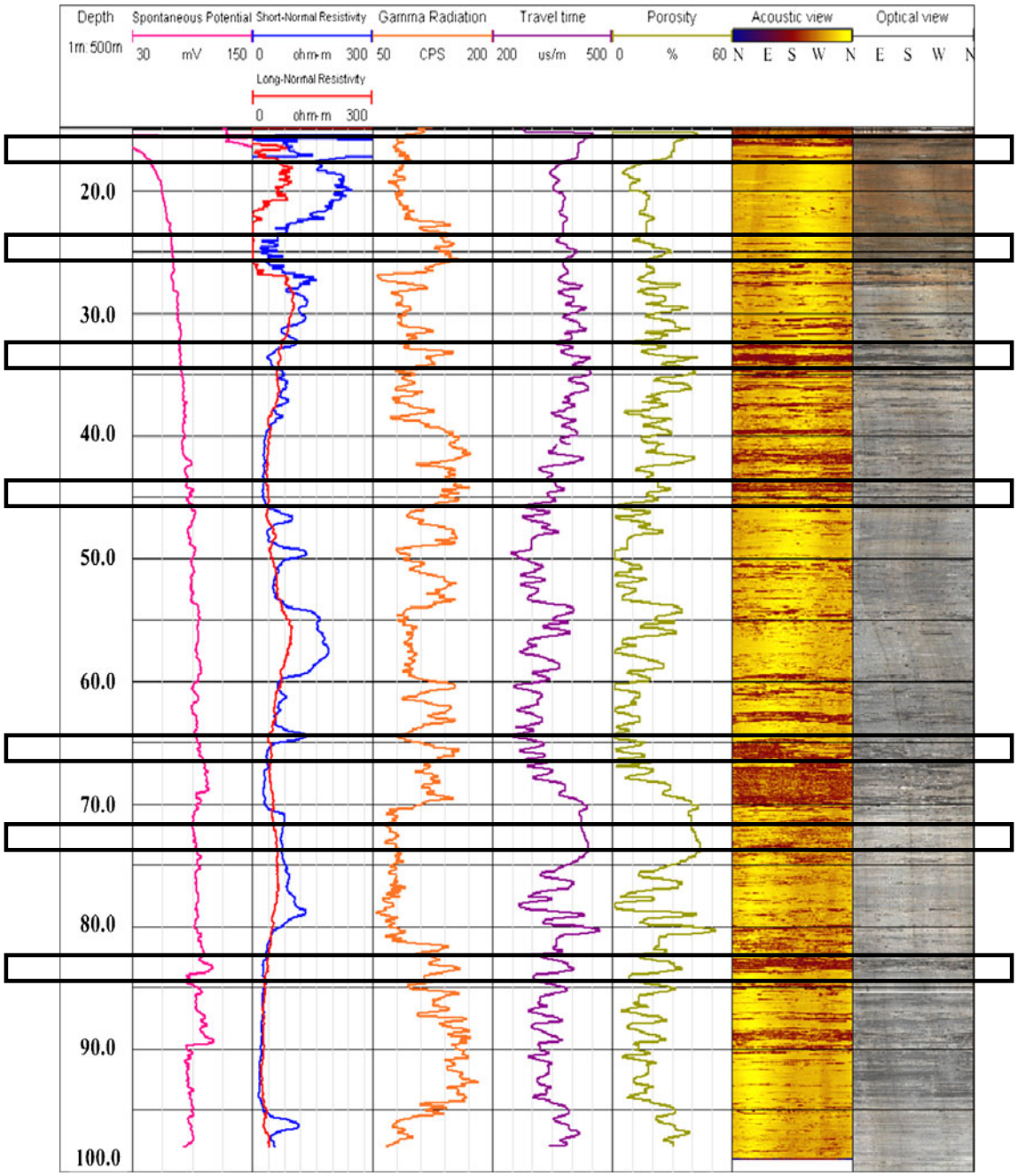


**Fig. 3** Geophysical log and televiewer profiles of borehole BH25

long one (here at depths of 15–40 m, 45 to 47 m, 48–51 m, 54–60 m, 63–65 m, 70–81 m, and 96–97 m) can be identified. It was confirmed by in-situ examination of core samples that these sections are primarily sandstone or sandy-siltstone dominated. In comparison with other shale-dominated sections, these seven sections are considered to potentially pose higher transmissivity.

– Sonic log: the reading of sonic travel-time shows a range from 250 to 450 μs/m ($V_L$ ranges from 4,000 to 2,222 m/sec). Since acoustic velocity in rock is porosity dependent, those segments with a relatively longer travel-time account for the occurrence of discontinuity spacing. It is presumed that the probable pathways are the long travel-time segments from the seven earlier-identified sections.
– Televiewer imaging: a continuous borehole image is clearly shown and the precise lithostratigraphic sequence can be mapped. The appearance of dark patches along the profile is an indication of loose-fillings or fracture zone. As a consequence, the efficacious pathway of groundwater flow can be identified by cross-matching the readings of geophysical logs and core inspection.


DOI 10.1007/s10040-012-0861-3

Based on the geophysical log and borehole televiewer profiles of borehole BH25, and with reference to experience in the authors' previous studies, four criteria have been tested for the prediction of hydraulically transmissive fractures, as follows:

I. *Lower gamma-ray response compared with the average response*

Since the natural gamma-ray log characterizes the radioactivity emanating from the rock surrounding the borehole, which is primarily related to the rock type and the concentration of clay minerals in the formation, typically, high gamma-ray response indicates the presence of fine-grained deposits or clay-rich rock formation, such as shale, claystone, mudstone, while relatively low gamma radiation indicates the presence of coarse-grained sandstone and carbonate rock, which exhibits higher transmissivity. Therefore, the satisfaction of the first criterion could confirm the presence of coarse-grained rock with relatively low concentration of clay minerals.

II. *Divergence of the short normal-resistivity log relative to that of the long one*

Since a deflection of short-normal log relative to the long one could attribute to the invention of drilling mud (Ellis and Ross 2007), and permeable zones could be identified by comparing the short normal-resistivity log relative to the long one (Helm-Clark et al. 2004), the satisfaction of the second criterion could imply the presence of permeable strata.

III. *Longer sonic travel time and/or larger porosity derived from acoustic velocity*

The sonic travel time of compressional waves through the formation correlates with the rock strength, elastic properties of formation, and most significantly, the lithological porosity. Typically, longer travel time is associated with the presence of larger porosity fractured bedrock. In other words, the concern of the third criterion could indicate the higher porosity and water-bearing layer.

IV. *Appearance of discernible openings from the televiewer (fractured zone)*

The use of televiewer logs allows a direct visual inspection of formation lithology to be made, so that all sorts of structural discontinuities intersecting the borehole wall can be recognized. Since most of fractures were commonly sealed with precipitated mineral cements, the satisfaction of the fourth criterion is to make sure that fractured media with discernible openings are identified. Furthermore, a cross-reference can be made with the driller's logs and rock core inspection.

In the light of these four criteria, a priori prediction of conductible segments can be made. Seven specific segments of discontinuity in borehole BH25 (as framed in Fig. 3 and listed in Table 2) are selected for the purpose of comparisons that scored by the four previously mentioned criteria.

As shown in Table 2, four segments, at the depths of 15.9–17.4, 24.0–25.5, 32.7–34.2 and 64.7–66.2 m, meet at least three out of four afore-mentioned criteria. One can reasonably presume that these four segments are prone to be more hydraulically transmissive than others. A comparison among different conductive sections with a conceptual sketch of the relevant attributes can be seen in Fig. 4.

## Hydraulic injection packer testing

After a continuous profile of the lithostratigraphic characteristics in each borehole has been identified, the hydraulic packer test can be performed to determine the transmissivity of those fractures that are presumed to be conductible. Since the application of the injection (Lugeon) tests with a single packer alone may only provide limited information, a double-packer system is employed. This technique has been widely employed elsewhere to determine the hydraulic properties of a fractured stratum (e.g. Morin et al. 1988; Howard et al. 1992; Brown and Slater 1999; Niemi et al. 2000; Ku et al. 2009; Mejías et al. 2009). As mentioned by Batu (1998), the principal concept of this technique involves the instantaneous pressurization of the test section and holding it constant over the test period; thereafter one can monitor and record the variation of injected flow rate (and/or pressure) over time. The detailed apparatus of the double packer assemblies employed in this study were described by Ku et al. (2009), and the testing procedures followed the American Society for Testing and Materials (ASTM) methods.

**Table 2** Quick identification of conductible segments in borehole BH25

| Depth of interval (m) | Criterion | | | | Predominate lithologic type |
|---|---|---|---|---|---|
| | I | II | III | IV | |
| 15.9–17.4 | b | b | b | b | Regolith (saprock) |
| 24.0–25.5 | a | b | b | b | Shale |
| 32.7–34.2 | a | b | b | b | Sandstone/shale interbedding |
| 43.9–45.4 | a | a | a | b | Sandstone/shale interbedding |
| 64.7–66.2 | b | b | a | b | Sandstone |
| 72.5–74.0 | b | a | b | a | Sandstone (mud-filled) |
| 82.5–84.0 | a | a | a | a | Sandstone (mud-filled) |

[a] Criteria is not satisfied

[b] Criteria is satisfied


DOI 10.1007/s10040-012-0861-3

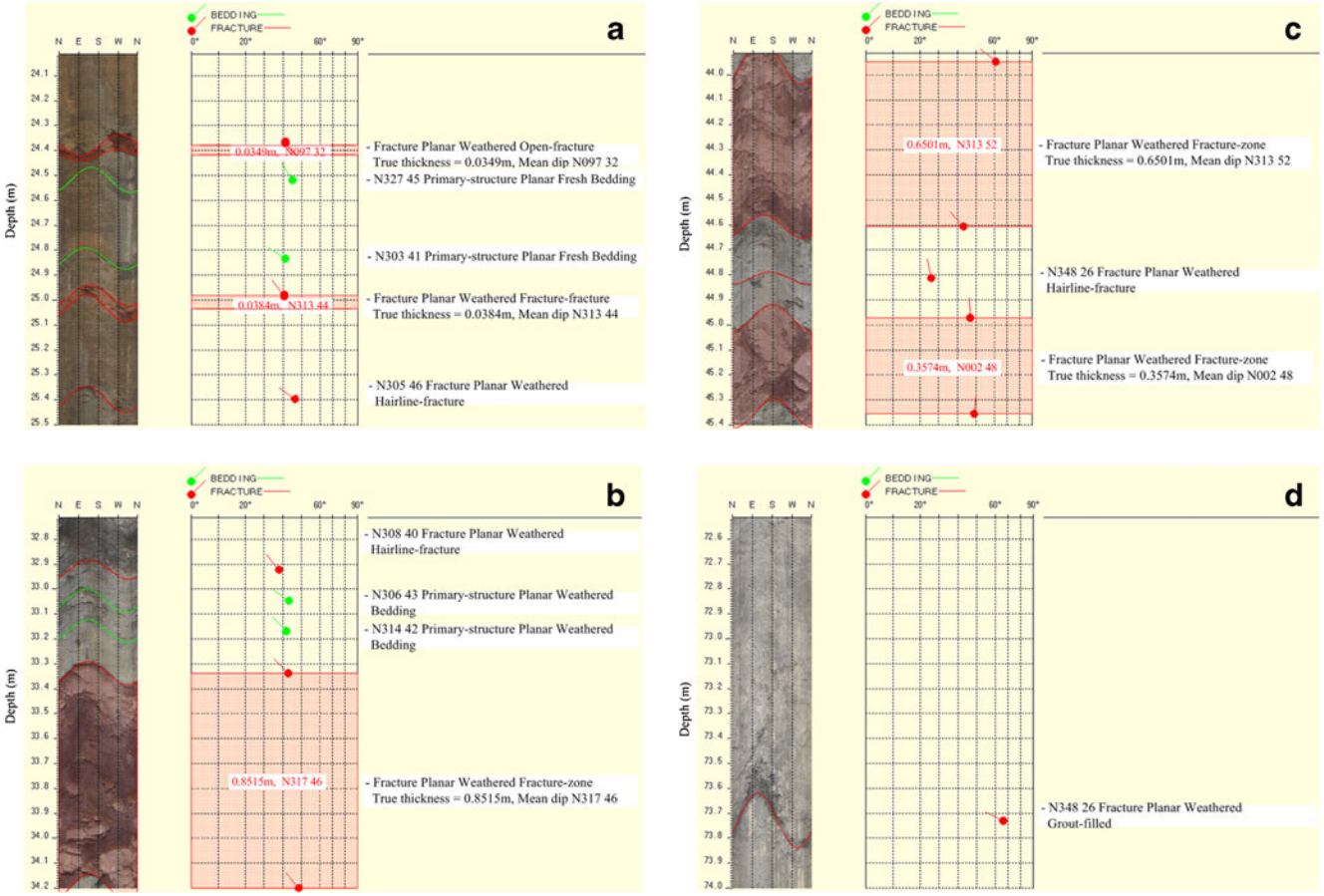


**Fig. 4** Comparison among different conductive sections with conceptual sketch of the relevant attributes of borehole BH25 at the depths of **a** 24.0–25.5 m; **b** 32.7–34.2 m; **c** 43.9–45.4 m; **d** 72.5–74.0 m

Using 29 boreholes, in total 158 test sections in consolidated bedrock were evaluated to determine the transmissivity. During the evaluation, each test started by applying the Constant Head Injection Test (CHIT) (on the basis of ASTM D4630-96 2002), which needs to ensure a volume of pressurized water to stably pass through the test section for a prolonged period of time. A constant water-flow injection rate is therefore essential for the interpretation of the test data. However, if no water flow was observed, then a logical and rational explanation is that this test section has a very low productivity ($T<10^{-9}$ $m^2$/sec). In such case, the CHIT method can no longer be used (no available water flow rate data), and an alternative hydraulic test method has to be performed, for instance the pressure pulse technique (PPT).

The equipment was cautiously calibrated in the laboratory and in the field. After the rubber packers were inflated with nitrogen gas delivered from a cylinder, the test section was completely sealed at top and bottom. The sealed-off interval in the current study was fixed at 1.5 m. Water was injected with a constant pressure of 0.2 MPa for the consideration of not causing irreparable damage to the aquifer. At least two test sections were specified in each borehole. In order to keep the borehole stable, and to diminish the risk of failure due to sloughing or spalling, testing was carried out from the section at the lowest position of the borehole and moving upward to the next. Each test took at least 3 h including rig transfer, quick calibration, packer inflation, data recording and pressure recovery. The variation of hydraulic head and injected flow rate within the testing section were recorded per second and stored in a data-logger developed by Sinotech Engineering Consultants Inc.

## Interpretation of hydraulic tests

Since the focus, and the objective, in the present study is on the prediction of hydraulically transmissive fractures, the present discussion is concerned only with those test sections that were tested by means of CHIT. Over the 158 test sections, only 67 were found in which a steady flow rate could be maintained. These 67 test sections were considered to be the primary hydraulically transmissive zones and assessed according to the criteria I-IV (Table 3). Within this group of interest, 53 with discernible openings were identified to be the fractured media; the 14 that remained intact were the non-fractured porous blocks.

Transmissivity was determined through the interpretation of injected flow rate by means of the software AQTESOLV, version 4.5 (HydroSOLVE Inc. Reston,


DOI 10.1007/s10040-012-0861-3

**Table 3** Stratigraphic log and transmissivity of test section

| Borehole code | Depth (m) | Gamma response (cps) | Short-normal resistivity (Ω-m) | Sonic derived porosity (%) | Fractured media (aperture, m)/ or non-fractured porous block | Rock type | Inclusion criteria | *n* | Transmissivity ($m^2$/sec) |
|---|---|---|---|---|---|---|---|---|---|
| BH02 | 51.2–52.7 | 155.5 | 22.7 | 11.08 | Fractured media (0.131) | Shale [S] | III, IV | 2.0 | 3.52E-08 |
| BH04 | 22.0–23.5 | 100.2 | 44.5 | 56.05 | Fractured media (0.805) | Sandstone [S] | III, IV | 2.6 | 4.79E-05 |
| BH06 | 40.6–42.1 | 91.3 | 68.6 | 28.70 | Fractured media (0.173) | Sandstone [S] | IV | 2.0 | 1.79E-07 |
| BH08 | 26.5–28.0 | 141.0 | 39.8 | 31.48 | Non-fractured porous block | Sandstone [S] | III | 2.0 | 3.42E-06 |
| BH08 | 42.0–43.5 | 109.0 | 82.3 | 31.60 | Fractured media (0.854) | Sandstone/shale [S] | III, IV | 2.0 | 1.07E-05 |
| BH08 | 66.0–67.5 | 99.4 | 131.8 | 16.79 | Non-fractured porous block | Sandstone [S] | - | 2.0 | 2.79E-07 |
| BH08 | 84.0–85.5 | 118.1 | 55.2 | 16.73 | Non-fractured porous block | Sandstone/shale [S] | - | 2.0 | 1.68E-08 |
| BH09 | 65.4–66.9 | 116.1 | 22.5 | 12.40 | Fractured media (0.968) | Sandstone [S] | IV | 2.0 | 1.98E-07 |
| BH10 | 23.0–24.5 | 84.0 | 654.1 | 11.60 | Fractured media (<0.001) | Quartzite [M] | I, III, IV | 3.0 | 4.75E-06 |
| BH10 | 57.1–58.6 | 76.9 | 792.9 | 18.44 | Fractured media (0.670) | Quartzite [M] | III, IV | 2.2 | 5.14E-08 |
| BH10 | 82.5–84.0 | 72.6 | 1568.7 | 13.75 | Fractured media (<0.001) | Quartzite [M] | I, II, III, IV | 3.0 | 3.22E-05 |
| BH11 | 54.0–55.5 | 173.9 | 341.6 | 19.97 | Non-fractured porous block | Slate [M] | III | 2.1 | 3.36E-07 |
| BH11 | 61.0–62.5 | 151.0 | 607.5 | 11.98 | Non-fractured porous block | Slate [M] | I, III | 2.0 | 2.66E-08 |
| BH11 | 88.0–89.5 | 138.4 | 1402.2 | 6.79 | Non-fractured porous block | Slate [M] | I | 2.0 | 2.47E-07 |
| BH12 | 22.7–24.2 | 56.5 | 5395.5 | 57.94 | Fractured media (0.326) | Quartzite [M] | II, III, IV | 3.0 | 2.96E-05 |
| BH12 | 42.0–43.5 | 121.2 | 2258.6 | 78.35 | Fractured media (0.291) | Quartzite [M] | I, III, IV | 2.3 | 1.14E-04 |
| BH12 | 53.0–54.5 | 140.7 | 1602.2 | 74.28 | Fractured media (<0.001) | Quartzite [M] | III, IV | 3.0 | 2.48E-05 |
| BH12 | 67.0–68.5 | 146.0 | 2639.8 | 46.69 | Fractured media (0.090) | Quartzite [M] | III, IV | 2.3 | 7.48E-07 |
| BH13 | 15.9–17.4 | 169.9 | 1942.4 | 58.97 | Non-fractured porous block | Slate [M] | III | 3.0 | 8.82E-06 |
| BH13 | 35.0–36.5 | 36.1 | 2684.7 | 58.32 | Non-fractured porous block | Quartzite [M] | II, III | 2.0 | 9.46E-07 |
| BH13 | 71.3–72.8 | 172.5 | 1428.5 | 52.32 | Fractured media (0.162) | Slate [M] | I, III, IV | 3.0 | 9.25E-06 |
| BH13 | 85.0–86.5 | 182.1 | 1641.4 | 28.64 | Fractured media (<0.001) | Slate [M] | III, IV | 2.5 | 3.61E-05 |
| BH15 | 33.0–35.0 | 87.0 | 77.7 | 40.24 | Non-fractured porous block | Sandstone [S] | II, III | 2.7 | 7.17E-08 |
| BH16 | 24.0–25.5 | 110.5 | 34.1 | 15.11 | Fractured media (0.145) | Sandstone [S] | IV | 3.0 | 1.40E-07 |
| BH16 | 36.1–37.6 | 107.3 | 61.4 | 21.04 | Fractured media (0.516) | Sandstone [S] | IV | 3.0 | 1.26E-06 |
| BH16 | 74.6–76.1 | 76.0 | 160.9 | 21.82 | Fractured media (1.169) | Sandstone [S] | IV | 2.0 | 1.82E-08 |
| BH16 | 84.5–86.0 | 108.2 | 56.8 | 11.24 | Fractured media (0.096) | Sandstone [S] | IV | 2.0 | 2.65E-05 |
| BH18 | 38.8–40.3 | 102.1 | 109.1 | 34.38 | Fractured media (1.490) | Sandstone [S] | II, III, IV | 2.2 | 1.85E-04 |
| BH18 | 49.0–50.5 | 97.8 | 186.5 | 10.15 | Fractured media (0.015) | Sandstone [S] | I, II, IV | 2.5 | 1.13E-04 |
| BH18 | 64.3–65.8 | 149.7 | 24.2 | 16.08 | Fractured media (0.262) | Shale [S] | III, IV | 2.0 | 2.73E-05 |
| BH18 | 75.5–77.0 | 110.3 | 24.3 | 37.75 | Fractured media (0.101) | Sandstone/shale [S] | III, IV | 2.3 | 2.24E-07 |
| BH19 | 24.9–26.4 | 82.2 | 174.1 | 34.33 | Fractured media (0.265) | Sandstone [S] | III, IV | 2.0 | 1.76E-06 |
| BH19 | 27.2–28.7 | 135.2 | 102.8 | 27.20 | Non-fractured porous block | Sandstone/shale [S] | III | 2.4 | 4.81E-06 |
| BH19 | 31.0–32.5 | 91.1 | 99.6 | 43.04 | Non-fractured porous block | Sandstone/shale [S] | II, III | 2.0 | 3.17E-07 |
| BH19 | 37.3–38.8 | 96.8 | 109.3 | 7.91 | Fractured media (0.100) | Sandstone/shale [S] | IV | 3.0 | 2.12E-07 |
| BH19 | 40.5–42.0 | 101.7 | 94.3 | 5.60 | Non-fractured porous block | Sandstone/shale [S] | II | 2.0 | 1.74E-06 |
| BH20 | 43.5–45.0 | 72.4 | 168.3 | 58.71 | Fractured media (0.570) | Sandstone [S] | I, II, III, IV | 2.1 | 2.75E-05 |
| BH20 | 54.0–55.5 | 84.3 | 217.7 | 31.14 | Fractured media (0.195) | Sandstone [S] | III, IV | 2.7 | 4.07E-05 |
| BH20 | 86.5–88.0 | 92.7 | 183.0 | 23.12 | Fractured media (0.398) | Sandstone [S] | IV | 2.0 | 4.53E-06 |
| BH21 | 32.1–33.6 | 153.2 | 1821.3 | 9.39 | Fractured media (<0.001) | Quartzite [M] | I, II, IV | 3.0 | 5.55E-05 |
| BH21 | 43.5–45.0 | 149.3 | 831.4 | 47.63 | Fractured media (0.901) | Quartzite [M] | I, III, IV | 3.0 | 5.60E-05 |
| BH21 | 50.3–51.8 | 141.4 | 653.0 | 8.63 | Fractured media (0.504) | Quartzite [M] | I, III, IV | 2.0 | 1.25E-05 |
| BH21 | 67.5–69.0 | 152.4 | 782.0 | 3.82 | Fractured media (0.241) | Quartzite [M] | IV | 3.0 | 1.68E-06 |
| BH21 | 83.3–84.8 | 146.7 | 1062.7 | 7.41 | Non-fractured porous block | Quartzite [M] | I | 2.5 | 6.04E-07 |
| BH21 | 92.7–94.2 | 141.3 | 720.2 | 17.69 | Fractured media (0.483) | Quartzite [M] | III, IV | 2.4 | 9.97E-06 |
| BH22 | 16.5–18.0 | 76.4 | 514.4 | 40.56 | Fractured media (1.490) | Sandstone [S] | I, II, III, IV | 2.1 | 1.60E-04 |
| BH22 | 24.2–25.7 | 69.5 | 600.5 | 15.57 | Fractured media (0.652) | Sandstone [S] | I, II, IV | 2.1 | 1.57E-05 |
| BH22 | 31.5–33.0 | 99.1 | 254.7 | 25.41 | Fractured media (0.474) | Sandstone [S] | IV | 2.9 | 3.18E-06 |

DOI 10.1007/s10040-012-0861-3

**Table 3** (continued)

| Borehole code | Depth (m) | Gamma response (cps) | Short-normal resistivity (Ω-m) | Sonic derived porosity (%) | Fractured media (aperture, m)/ or non-fractured porous block | Rock type | Inclusion criteria | *n* | Transmissivity ($m^2$/sec) |
|---|---|---|---|---|---|---|---|---|---|
| BH22 | 39.5–41.0 | 104.7 | 185.5 | 24.13 | Fractured media (0.858) | Sandstone [S] | IV | 2.0 | 6.49E-07 |
| BH22 | 47.2–48.7 | 90.1 | 343.1 | 7.19 | Fractured media (0.383) | Sandstone [S] | IV | 3.0 | 2.85E-07 |
| BH22 | 70.5–72.0 | 110.9 | 425.2 | 3.43 | Non-fractured porous block | Sandstone [S] | - | 3.0 | 3.57E-07 |
| BH22 | 85.0–86.5 | 94.3 | 393.3 | 13.06 | Fractured media (<0.001) | Sandstone [S] | IV | 2.1 | 1.59E-07 |
| BH23 | 17.5–19.0 | 139.1 | 97.0 | 29.65 | Fractured media (0.362) | Sandstone [S] | I, III, IV | 3.0 | 4.92E-05 |
| BH23 | 27.3–28.8 | 149.7 | 90.4 | 17.70 | Fractured media (0.122) | Sandstone [S] | III, IV | 3.0 | 1.22E-05 |
| BH23 | 41.0–42.5 | 124.6 | 89.7 | 15.45 | Fractured media (0.663) | Sandstone [S] | III, IV | 3.0 | 2.71E-05 |
| BH23 | 47.6–49.1 | 122.8 | 106.4 | 12.73 | Fractured media (0.657) | Sandstone [S] | III, IV | 3.0 | 9.13E-06 |
| BH23 | 72.0–73.5 | 144.5 | 101.0 | 4.53 | Fractured media (0.096) | Sandstone [S] | III, IV | 3.0 | 1.50E-05 |
| BH23 | 86.5–88.0 | 125.1 | 156.2 | 4.32 | Fractured media (0.022) | Sandstone [S] | I, II, III, IV | 2.9 | 5.99E-05 |
| BH24 | 17.7–19.2 | 102.2 | 94.2 | 16.79 | Fractured media (<0.001) | Sandstone [S] | I, II, IV | 3.0 | 5.20E-05 |
| BH24 | 23.0–24.5 | 80.3 | 93.4 | 18.62 | Fractured media (<0.001) | Sandstone [S] | I, II, IV | 2.7 | 9.95E-06 |
| BH25 | 24.0–25.5 | 141.6 | 42.9 | 21.83 | Fractured media (0.073) | Shale [S] | II, III, IV | 2.0 | 1.02E-05 |
| BH25 | 32.7–34.2 | 123.2 | 52.3 | 25.67 | Fractured media (0.852) | Sandstone/shale [S] | II, III, IV | 2.9 | 3.03E-04 |
| BH25 | 43.9–45.4 | 150.4 | 27.4 | 22.39 | Fractured media (1.007) | Sandstone/shale [S] | III, IV | 3.0 | 3.96E-07 |
| BH25 | 64.7–66.2 | 129.3 | 53.5 | 9.84 | Fractured media (1.237) | Sandstone [S] | I, II, IV | 2.8 | 2.47E-06 |
| BH25 | 82.5–84.0 | 135.4 | 28.7 | 25.51 | Fractured media (0.533) | Sandstone [S] | IV | 2.0 | 1.09E-07 |
| BH26 | 49.5–51.0 | 135.8 | 83.5 | 12.11 | Fractured media (0.779) | Sandstone [S] | IV | 2.7 | 3.80E-07 |
| BH27 | 12.5–14.0 | 122.3 | 63.3 | 16.50 | Fractured media (0.188) | Shale [S] | III, IV | 2.0 | 8.18E-07 |

*S* sedimentary rock; *M* metamorphic rock

VA). AQTESOLV can be considered as one of the most applied software in the field of hydrogeology for the determination of hydraulic conductivity, and offers a variety of analytical solutions for not only virtual but also automatic type curve matching to facilitate interpretation. Recently, this software has been adopted in the hydrogeological studies of fractured rock aquifers by Maréchal et al. (2004), Muldoon and Bradbury (2005), Verbovšek (2009), and Chang et al. (2011).

The generalized radial flow (GRF) model proposed by Barker (1988) was adopted in the current study. This model has been widely applied in practice with success for the interpretation of hydraulic tests. The fundamental assumptions of the GRF model are: the flow is radial, the fractured medium is homogeneous and isotropic, skin thickness is infinitesimal, and Darcy's law is valid. The GRF model accounts for the multi-scale fracture network heterogeneity (Le Borgne et al. 2004). As pointed out by Cloot and Botha (2006) and Cello et al. (2009), the aquifer geometry in a GRF model is assumed to be a fractal network of conduits, which meets the actual geological condition of this study area in Taiwan. This model is written as:

$$S_s \frac{\partial h}{\partial t} = \frac{K}{r^{n-1}} \frac{\partial}{\partial r}\left(r^{n-1} \frac{\partial h}{\partial r}\right) \qquad \text{(Eq.2)}$$

where $S_s$ represents the specific storage of the aquifer [1/L] and it has been bounded within $10^{-6}$ to 1 ($m^{-1}$); $h(r, t)$ denotes the change in hydraulic head [L] with time, $r$ represents the radial distance from the borehole [L]; $K$ represents the hydraulic conductivity [L/T]; $n$ denotes the flow dimension (i.e. the change of the cross-sectional area to the flow) according to the distance from the borehole (Walker and Roberts 2003). This parameter has been bounded, according to the suggestion of Kuusela-Lahtinen et al. (2003) for the fractal assumptions, with 2, for cylindrical flow and 3, for spherical flow. One example of experimental data obtained by CHIT and the evaluation using AQTESOLVE is illustrated in Fig. 5.

In Table 3, the geophysical attributes and hydraulic conditions of the 67 test sections that have been determined as hydraulically transmissive zones are presented in terms of the corresponding depth, gamma response, resistivity, sonic-derived porosity, fractured media with aperture or non-fractured porous block, rock type, inclusion criteria, flow dimension ($n$), and the estimated transmissivity ($T=K\times1.5^{(3-n)}$).

## Results and discussion

### Estimation of transmissivity

As shown in Table 3, for all test sections that were capable of being tested by CHIT, 47 were found in the sedimentary rocks and only 20 in the metamorphic rocks. If only the fractured media are considered, the majority were identified in the sedimentary rocks, accounting for


DOI 10.1007/s10040-012-0861-3

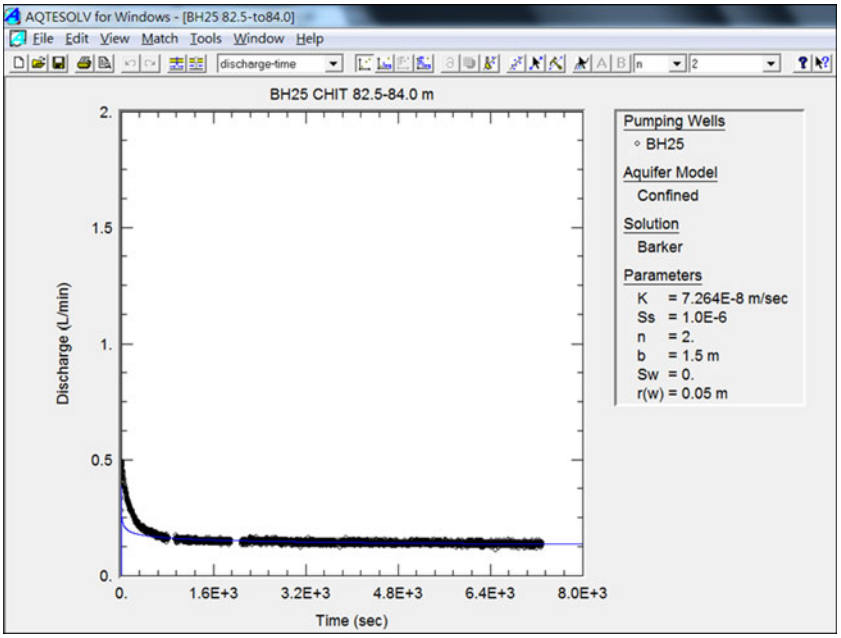


**Fig. 5** Example of one experimental dataset obtained by CHIT and the evaluation using AQTESOLVE

about 74 % of the total discernible fracture population. Comparatively, a lesser amount of hydraulically transmissive fractured media was found in the metamorphic rocks. This could be due to the fact that the porosity of metamorphic rocks is low and vein-filling mineral assemblages (such as micas and quartz) are presented, thereby, the groundwater flow is restricted only to some portions of the domain. In spite of this, with regard to the distribution of flow dimension in the metamorphic rock, most of the identified test sections are found to be intersected with a dense fracture network ($n>2$).

With a view to evaluate the transmissivity of fractured media and non-fractured porous block, the values of transmissivity determined from CHIT are plotted on a logarithmic scale, as shown in Fig. 6, against depth on a linear scale. The corresponding cross plot between transmissivity and the type of rock is also presented.

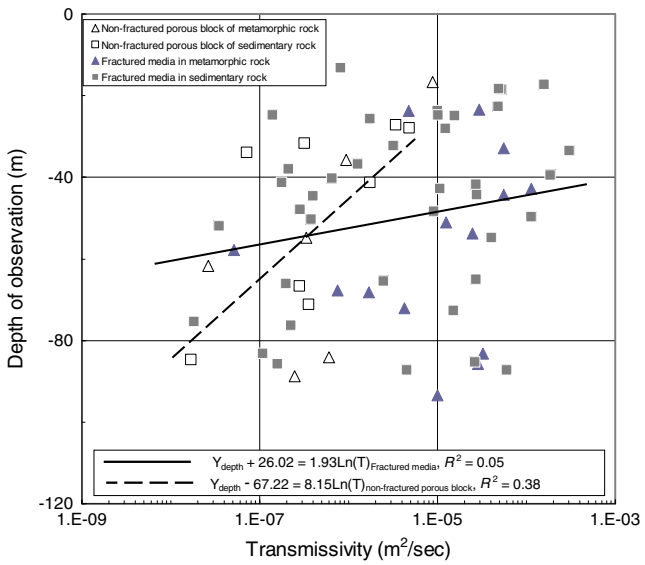


**Fig. 6** Plot of the estimated transmissivity on a logarithmic scale with respect to different types of rock against depth in borehole

From a broad-scale perspective, based on the geometric means of transmissivity data, the transmissivity of fractured media ($4.85\times10^{-6}$ m$^2$/sec) is approximately a factor of 11 higher than that of non-fractured porous block ($4.45\times10^{-7}$ m$^2$/sec); while if only the fractured media are considered, a relatively higher transmissivity ($9.2\times10^{-6}$ m$^2$/sec) above a depth of 40 m (i.e. the upper part of bedrock lying beneath the regolith layer) is obtained in comparison with that at the greater depth ($3.3\times10^{-6}$ m$^2$/sec). These can be assigned as the representative initial values for the construction of a conceptual hydrogeological model in a later stage. A further subdivision can be made in terms of the magnitude of transmissivity as follows: (1) high-transmissive medium: $T \geqq 1\times10^{-5}$ m$^2$/sec, (2) semi-transmissive medium $1\times10^{-5}>T\geqq 5\times10^{-7}$ m$^2$/sec; (3) low-transmissive medium $T<5\times10^{-7}$ m$^2$/sec.

Unlike a number of previous studies that concluded a power relationship (Chappell and Lancaster 2007), or an exponential decay (Saar and Manga 2004; Jiang et al. 2009) in transmissivity with depth, no significant correlation between depth and transmissivity was found in this study. Taking account of experience from previous studies (Krásný 2002; Taylor and Howard, 1999; 2000; Morin and Savage, 2003; Maréchal et al. 2004; Dewandel et al. 2006; Lachassagne et al. 2009; 2011), a possible interpretation for the inconsistency is that the occurrence of a secondary fracture set contributes to the increase in transmissivity, and which is the result of tectonic stress, stripping or deep weathering. This suggests that to establish a conceptual hydrogeological model for this study area, rather than assigning depth-dependent-transmissivity in multiple layers, it could be more appropriate to specify site-specific transmissivity values for different depth domains.


DOI 10.1007/s10040-012-0861-3

A simple statistical comparison for the effective transmissivity (within the range bounded by the arithmetic and harmonic means) at different depths can be seen in Table 4. Based on the results of in situ hydraulic tests, the upper part of the bedrock possesses high-to-semi transmissive capacity, while the lower part (40–100 m) of the bedrock exhibits a wide range in transmissivity (high-to-low). A similar trend can also be found by respectively comparing the transmissivity estimates of metamorphic rock and of sedimentary rock. Additionally, though only a few test sections in metamorphic rocks were capable of being tested by CHIT, their effective transmissivity appeared to be consistently high. As shown in Table 4, for the range from 0 to 40 m, the effective transmissivity in metamorphic rock is $1.99\times10^{-5}$ to $3.49\times10^{-6}$ $m^2$/sec; comparatively, a greater variance of effective transmissivity in sedimentary rocks, $4.10\times10^{-5}$ to $6.12\times10^{-7}$ $m^2$/sec, is shown.

## Explorative data analysis

A cross-plot of the natural-gamma responses and short-normal resistivity logs (with logarithmic scale) is shown in Fig. 7, in which the distinction in terms of the surrounding bulk rock types is also presented. It can be seen that clearly an inverse relation exists between natural-gamma responses and electrical resistivities. As indicated by the study of Morin et al. (2000), such interdependence is closely related to the grain size: the coarse-grained dominant rocks tend to exhibit a higher resistivity but lower gamma response, and vice versa. Correspondingly, the electrical resistivity of metamorphic rocks is found to be approximately one order higher than the resistivities of sedimentary rocks.

One can recognize the discrimination in accordance with the corresponding transmissivity of each test section in Fig. 7, but it is hard to directly correlate the logs of natural-gamma responses and short-normal resistivity to the magnitude of transmissivity. This is attributed to the fact that the occurrence of groundwater in the network of fractures is not solely governed by lithological attributes but more on fracture network properties.

In addition to the porosity of the rock, the most essential geometric property of a fractured rock aquifer is the open-fracture aperture, which is capable of being measured in situ from the televiewer imagines with no need of further laboratory testing. In order to reveal the correlation of transmissivity with the sonic-derived porosity and fracture aperture, an "aperture ratio" is defined as the division of the "sum of all individual open fracture-apertures" by the "sealed-off interval between the packers", which leads to a rational approach to the prediction of fracture transmissivity once different lengths of test interval are applied. Accordingly, those fine hairline-cracks with aperture less than 1 mm are not taken into account, since their apertures are too thin to be measured.

When considered individually, it was found that the correlation of transmissivity to the sonic derived porosity (Pearson's $r=0.25$), and the correlation of transmissivity to the aperture ratio (Pearson's $r=0.34$), are weak. Interestingly, as it can be seen in Fig. 8, a slightly stronger correlation (Pearson's $r=0.42$) is shown when plotting the transmissivities versus the product of porosity and aperture ratio. This correlation suggests that if the two primary fracture-network characteristics, i.e. the intra-aggregate pores and the inter-aggregate voids, could be taken into consideration simultaneously, the accuracy in the prediction of fracture transmissivity might be increased. In other words, for an internally consistent geological formation associated with uniform porosity distribution, the occurrence of high-transmissive zones is likely to locate in the range consisting of larger fracture openings; nevertheless, when respectively comparing the transmissivity of two individual fractured media within the geological formation where a hierarchical distribution of porosity is shown, those fractured media associated with larger inter-aggregate pore space shall be prone to becoming the preferential groundwater conduits.

## Cross comparison of criteria used for identifying conductible fractures

It is worthwhile to examine the predetermined criteria used for identifying conductible fractures. On the basis of the fulfillment of the four criteria, the upper and lower bounds of the estimates of transmissivity are presented in Fig. 9. The coefficient of variance (CV) of the log-transformed transmissivity is provided. Unpaired Student's *t*-test is also

**Table 4** The effective transmissivity (*T*) of test sections at different depths

| | | Metamorphic rock | Sedimentary rock |
|---|---|---|---|
| Depth at 0–40 m | | | |
| *T*-arithmetic | 3.70E-05 (high) | 1.99E-05 (high) | 4.10E-05 (high) |
| *T*-harmonic | 7.27E-07 (semi) | 3.49E-06 (semi) | 6.12E-07 (semi) |
| *T*-SD | 7.16E-05 | 2.28E-05 | 7.89E-05 |
| Number of data | 26 | 5 | 21 |
| Depth at 40–100 m | | | |
| *T*-arithmetic | 1.62E-05 (high) | 1.99E-05 (high) | 1.42E-05 (high) |
| *T*-harmonic | 1.59E-07 (low) | 2.20E-07 (low) | 1.37E-07 (low) |
| *T*-SD | 2.73E-05 | 3.10E-05 | 2.54E-05 |
| Number of data | 41 | 15 | 26 |

*T-arithmetic* Arithmetic mean of transmissivity ($m^2$/sec); *T-harmonic* Harmonic mean of transmissivity ($m^2$/sec); *T-SD* Standard deviation of data set


DOI 10.1007/s10040-012-0861-3

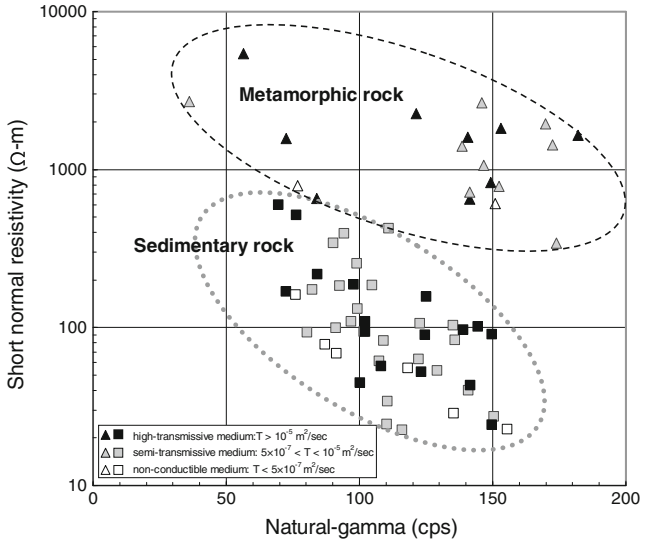


**Fig. 7** Cross-plot of natural-gamma values versus short-normal resistivity logs

employed to evaluate the significance of differences between each group (Table 5) according to the *P*-value ($\leq 0.05$).

For the test sections that fulfill all of the selection criteria (group A): i.e. contained discernible open fractures (criterion IV) along with low gamma-ray response (criterion I), intensified short normal-resistivity relative to the long one (criterion II), and longer sonic travel time (criterion III), a rather consistent pattern of high transmissivity ($T>10^{-5}$ m$^2$/sec, CV for log-$T$=0.12) is displayed. The identified fractures hereunder can be confidently regarded as the local primary conduits for groundwater flow.

For the test sections that meet three of the four criteria (group B to D), notwithstanding a greater scatter of estimates (CV for log-$T$=0.29~0.47), in comparison with group A, the *P*-value obtained by *t*-test between each pair

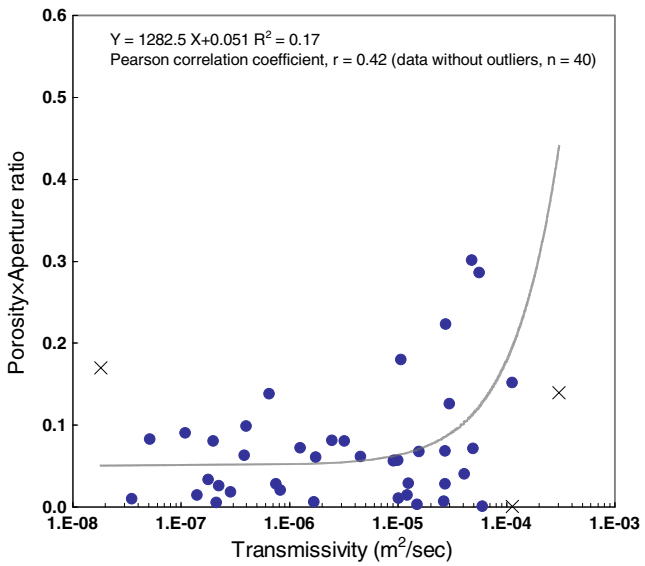


**Fig. 8** Transmissivity in the logarithm scale versus the product of sonic derived porosity and aperture ratio. The *x* represents the outliers

of groups is greater than 0.05, so the majority can still be classified as high-transmissive media. Obviously, the presence of a fracture zone in association with a longer sonic travel-time appears to be an essential prerequisite for the identification of the effective pathway. However, if the consideration of lithologic properties fails to satisfy the afore-mentioned criteria I and criteria II (group E and F), the estimates of fracture transmissivity are shown to exhibit considerable variability (CV for log-$T$=0.62 and 1.04) and significant differences (*P*-value is less or equal to 0.05). These two groups of open fractures may play a less significant role in controlling the local groundwater flow than the intra-aggregate pores.

The result indicates that, rather than carrying out various types of geophysical logging techniques, a careful comparison by means of the four previously mentioned criteria enables a priori accurate prediction of the highly transmissive fractures. Particularly in the study area, where a complex folded mountain structure with a succession of synclines and anticlines is shown, the lithologic interpretation is merely a sufficient criterion. In contrast, the estimates of porosity and fracture aperture are the necessary premises to the prediction of hydraulically transmissive fractures in such dual-porosity systems. A joint consideration of all afore- mentioned factors allows a less biased evaluation of the fracture transmissivity.

## Conclusions and recommendations

1. This paper aims to report the preliminary major findings, in terms of fracture transmissivity, of an investigation in the mountainous area of Jhuoshuei River basin, Taiwan. For the identification of hydraulically transmissive fractures, the analysis of geological/geophysical well-logging data and borehole televiewer data is the priority concern. It is also the purpose of this study to provide a theoretical and empirical based guideline for quick identification of hydraulically transmissive fractures, especially when the drilling project is constrained by limited budget and time.
2. Four hypothesized criteria that assist in indicating the potential presence of permeable zones are proposed, including (1) lower gamma-ray response compared with the average response, (2) divergence of the short normal-resistivity log relative to that of the long one, (3) longer sonic travel time, and (4) the appearance of discernible openings using the televiewer, whereby the transmissivity at the predetermined depths is estimated and verified by the in-situ hydraulic test.
3. Based on the geometric means of transmissivity data, the transmissivity of fractured media is found to be a factor of 11 times higher than that of non-fractured media. Above a depth of 40 m, a relatively higher transmissivity of fractured media is obtained, but the overall correlation between fracture transmissivity and depth of investigation is not significant. The effective transmissivity in metamorphic formations appears to be


DOI 10.1007/s10040-012-0861-3

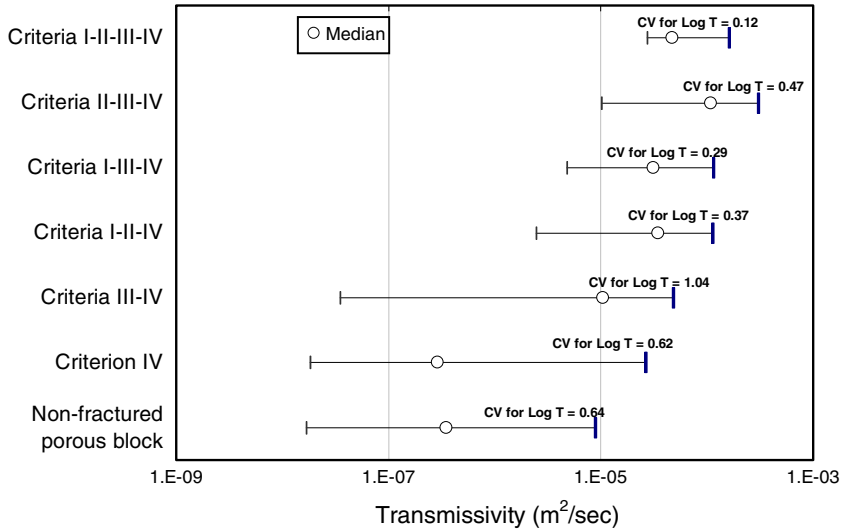


**Fig. 9** Comparison of the criteria for identifying hydraulically transmissive fractures

consistently high ($3.49\times10^{-6}$ ~$1.99\times10^{-5}$ $m^2$/sec), while the estimates in sedimentary formations show greater variance ($6.12\times10^{-7}$ ~$4.10\times10^{-5}$ $m^2$/sec). This accounts for the fact that the occurrence of fracture zones in metamorphic rock contributes as the predominant pathway for groundwater flow; in contrast, the fractures in sedimentary rock are often poorly connected and thus showing little effect on the overall permeability of the aquifer. Accordingly, rather than assigning depth-dependent-transmissivity in multiple layers, it is more appropriate to specify site-specific transmissivity in different depth domains when constructing a conceptual hydrogeological model for this study area.

4. For the majority of open fractures identified in this study, the increase in transmissivity is found to be associated with the product of sonic derived porosity and aperture ratio. Furthermore, the cross-comparison results of the four prefigured criteria show that, by considering the fracture geometries as the necessary premise and taking local lithologic interpretation into account, a priori accurate prediction of the highly transmissive fractures can be obtained. This allows one to characterise the spatial variation of permeability along a borehole simply relying on the use of geophysical logging and televiewer imaging.
5. In a heterogeneous mountainous environment with complex folded structures, not only the fracture aperture but also the porosity of formation may change dramatically. For gaining more insight and conclusive evidence regarding aquifer heterogeneity, the contribution from different local discontinuities (such as hairline-cracks or potholes) within the same geologic formation, as well as the corresponding flow dimension, deserves to be re-evaluated.

**Table 5** The results of *t*-test between each group

| | A | B | C | D | E |
|---|---|---|---|---|---|
| B | t-st: -0.197, df: 6, *P*-value: 0.425 | | | | |
| C | t-st: 1.174, df: 8, P -value: 0.137 | t-st: 1.127, df: 8, *P*-value: 0.146 | | | |
| D | t-st: 1.127, df: 8, *P*-value: 0.146 | t-st: 1.109, df: 8, *P*-value: 0.150 | t-st: 0.069, df: 10, *P*-value: 0.473 | | |
| E | t-st: 2.179, df: 20, *P*-value: 0.021* | t-st: 2.258, df: 20, *P*-value: 0.018* | t-st: 1.786, df: 22, *P*-value: 0.044* | t-st: 1.715, df: 22, *P*-value: 0.050* | |
| F | t-st: 5.003, df: 17, *P*-value: 5.45E-5** | t-st: 4.907, df: 17, *P*-value: 6.66E-5** | t-st: 4.802, df: 19, *P*-value: 6.20E-5** | t-st: 4.642, df: 19, *P*-value: 8.88E-5** | t-st: 2.809, df: 31, *P*-value: 0.004** |

*A* Sections fulfill selection criteria I, II, III, IV. The statistical mean of Log-T is −4.268

*B* Sections fulfill selection criteria II, III, IV. The statistical mean of Log-T is −4.193

*C* Sections fulfill selection criteria I, III, IV. The statistical mean of Log-T is −4.627

*D* Sections fulfill selection criteria I, II, IV. The statistical mean of Log-T is −4.650

*E* Sections fulfill selection criteria III and IV only. The statistical mean of Log-T is −5.411

*F* Sections fulfill selection criterion IV only. The statistical mean of Log-T is −6.315

*t-st* t-statistics, df: degrees of freedom

**P*-value ≦ 0.05 (significant difference), ***P*-value <0.01 (very significant difference)

 DOI 10.1007/s10040-012-0861-3

6. For the tectonically active areas, such as this case in Taiwan, where a heterogeneous stress field has been suggested (Hsu et al. 2010), more systematic research is required to investigate the effect of variations in tectonic stress on the long-term productivity of the fractures. It is consequently recommended that the next research project should include additional data about the orientation of tectonic stress, so that influences on the local hydrogeological properties may be better understood.

**Acknowledgements** The authors are grateful for the comments and suggestions from the Editor, Dr. Jiu Jimmy Jiao, and the Associate Editor. The recommendations from Mr. Anders Winberg and the two anonymous reviewers are greatly appreciated. The authors are also grateful for the financial support of the Central Geological Survey, Ministry of Economic Affairs (MOEA) of Taiwan, and for the preparation of the geologic map of the study area by Mr. Jung-Jun (Alan) Lin.

## References

Barker JA (1988) A generalized radial flow model for hydraulic tests in fractured rock. Water Resour Res 24:1796–1804

Barton CA, Zoback MD, Moos D (1995) Fluid flow along potentially active faults in crystalline rock. Geology 23:683–686

Batu V (1998) Aquifer hydraulics: a comprehensive guide to hydrogeologic data analysis. Wiley, New York

Becker MW, Shapiro AM (2000) Tracer transport in fractured crystalline rock: evidence of nondiffusive breakthrough tailing. Water Resour Res 36:1677–1686

Bense VF, Van Balen RT, De Vries JJ (2003) The impact of faults on the hydrogeological conditions in the Roer Valley Rift System: an overview. Neth J Geosci 82:41–53

Brown D, Slater LD (1999) Focused packer testing using geophysical tomography and CCTV in a fissured aquifer. Q J Eng Geol Hydrogeol 32:173–183

Cello P, Walker DD, Valocchi AJ, Loftus B (2009) Flow dimension and anomalous diffusion of aquifer tests in fracture networks. Vadose Zone J 8:258–268

Chang YC, Yeh HD, Liang KF, Kuo MCT (2011) Scale dependency of fractional flow dimension in a fractured formation. Hydrol Earth Syst Sci 15:2165–2178

Chappell NA, Lancaster JW (2007) Comparison of methodological uncertainty within permeability measurements. Hydro Proc 21:2504–2514

Chapellier D (1992) Well logging in hydrogeology. Balkema, Brookfield, MA, p 175

Chia Y, Wang YS, Chiu JJ, Lui CW (2001) Changes of groundwater level due to the 1999 Chi-Chi earthquake in the Choshui River Alluvial Fan in Taiwan. B Seismol Soc Am 91:1062–1068

Chow JJ, Lee MG, Fhu SC (2005) Geophysical well log study on the paleoenvironment of the hydrocarbon producing zones in the Erchungchi formation, Hsinyin, SW Taiwan. Terr Atmos Ocean 16:531–545

Cloot A, Botha JF (2006) A generalised groundwater flow equation using the concept of non-integer order derivatives. Water SA 32:1–7

Dewandel B, Lachassagne P, Wyns R, Maréchal JC, Krishnamurthy NS (2006) A generalized 3-D geological and hydrogeological conceptual model of granite aquifers controlled by single or multiphase weathering. J Hydrol 330:260–284

Doan ML, Brodsky EE, Kano Y, Ma KF (2006) In situ measurement of the hydraulic diffusivity of the active Chelungpu Fault, Taiwan. Geophys Res Lett 33:L16317. doi:10.1029/2006GL026889

Ellis D, Ross TM (2007) A Summary of the Drilling and Completion of the Borrego Water district Monitoring Well MW-4 and Geophysical Observations and Initial Interpretations. California Department of Water Resources, Southern District Technical Information Record SD-07-02. Available via http://www.dpla.water.ca.gov/sd/groundwater/publications/TIR%20SD_07_03.pdf. Cited 15 Jan 2011

Guimerà J, Carrera J (1997) On the interdependence of transport and hydraulic parameters in low permeability fractured media. In: Proceedings of Rabat Symposium, Hard Rocks Hydrosystems, Morocco, May 1997, pp 123–133

Hall SH, Luttrell SP, Cronin WE (1991) A method for estimating effective porosity and ground-water velocity. Ground Water 29:171–174

Hamm SY, Kim MS, Cheong JY, Kim JY, Son M, Kim TW (2007) Relationship between hydraulic conductivity and fracture properties estimated from packer tests and borehole data in a fractured granite. Eng Geol 92:73–87

Helm-Clark CM, Rodgers DW, Smith RP (2004) Borehole geophysical techniques to define stratigraphy, alteration and aquifers in basalt. J Appl Geophys 55:3–38

Henriksen H (2006) Fracture lineaments and their surroundings with respect to groundwater flow in the bedrock of Sunnfjord, western Norway. Norweg J Geol 86:373–386

Howard KWF, Hughes M, Charlesworth DL, Ngobi G (1992) Hydrogeologic evaluation of fracture permeability in crystalline basement aquifers of Uganda. Hydrogeol J 1:55–65

Hsieh BZ, Lewis C, Lin ZS (2005) Lithology identification of aquifers from geophysical well logs and fuzzy logic analysis: Shui-Lin Area, Taiwan. Comput Geosci 31:263–275

Hsu YJ, Rivera L, Wu YM, Chang CH, Kanamori H (2010) Spatial heterogeneity of tectonic stress and friction in the crust: new evidence from earthquake focal mechanisms in Taiwan. Geophys J Int 182:329–342

Hubbard B, Roberson S, Samyn D, Merton-Lyn D (2008) Instruments and methods digital optical televiewing of ice boreholes. J Glaciol 54:823–830

Jiang XW, Wan L, Wang XS, Ge S, Liu J (2009) Effect of exponential decay in hydraulic conductivity with depth on regional groundwater flow. Geophys Res Lett 36:L24402. doi:10.1029/2009GL041251

Kaus BJP, Liu Y, Becker TW, Yuen DA, Shi Y, Hon JJ, Ye H (2009) Lithospheric stress-states predicted from long-term tectonic models: influence of rheology and possible application to Taiwan. J Asian Earth Sci 36:119–134

Keys WS (1990) Borehole geophysics applied to ground-water investigations. In: US Geol Surv Tech Water Resour Invest, book 2, chap. E2. Available via http://pubs.usgs.gov/twri/twri2-e2. Cited 15 Jan 2011

Krásný J (2002) Quantitative hardrock hydrogeology in a regional scale. Norgweg Geol Unders B 439:7–14

Ku CY, Hsu SM, Chiou LB, Lin GF (2009) An empirical model for estimating hydraulic conductivity of highly disturbed clastic sedimentary rocks in Taiwan. Eng Geol 109:213–223

Kuusela-Lahtinen A, Niemi A, Luukkonen A (2003) Flow dimension as an indicator of hydraulic behavior in site characterization of fractured rock. Ground Water 41:333–341

Lachassagne P, Ahmed S, Dewandel B, Courtois N, Maréchal JC, Perrin J, Wyns R (2009) Recent improvements in the conceptual model of hard rock aquifers and its application to the survey, management, modelling and protection of groundwater. In: Groundwater and climate in Africa. Proceedings of the Kampala Conference, Kampala, Uganda, June 2008, IAHS Publ. 334, IAHS, Wallingford, UK, pp 250–256)

Lachassagne P, Wyns R, Dewandel B (2011) The fracture permeability of hard rock aquifers is due neither to tectonics, nor to unloading, but to weathering processes. Terra Nova 23:145–161

Lau KC (1998) A review of downhole geophysical methods for ground investigation. Technical note no. TN 4/98, Geotechnical Engineering Office, Hong Kong. Available

via http://www.cedd.gov.hk/eng/publications/geo_reports/doc/er99.pdf. Cited 15 Jan 2011
Le Borgne T, Bour O, de Dreuzy JR, Davy P, Touchard F (2004) Equivalent mean flow models for fractured aquifers: insights from a pumping tests scaling interpretation. Water Resour Res 40:W03512. doi:10.1029/2003WR002436
Lee CF, Hon JJ, Ye H (1997) The movement potential of the major faults in Hong Kong area. Episodes 20:227–231
Maréchal JC, Dewandel B, Subrahmanyam K (2004) Use of hydraulic tests at different scales to characterize fracture network properties in the weathered-fractured layer of a hard rock aquifer. Water Resour Res 40:W11508. doi:10.1029/2004WR003137
Marine IW (1980) Determination of the location and connectivity of fractures in metamorphic rock with in-hole tracers. Ground Water 18:252–261
Matthäi SK (2003) Fluid flow and (reactive) transport in fractured and faulted rock. J Geochem Explor 78–79:179–182
McKay LD, Cherry JA, Gillham RW (1993) Field experiments in a fractured clay till: 1. Hydraulic conductivity and fracture aperture. Water Resour Res 29:1149–1162
Mejías M, Renard P, Glenz D (2009) Hydraulic testing of low-permeability formations: a case study in the granite of Cadalso de los Vidrios, Spain. Eng Geol 107:88–97
Morin RH (2005) Hydrologic properties of coal beds in the Powder River Basin, Montana I: geophysical log analysis. J Hydrol 308:227–241
Morin RH, Savage WZ (2003) Effects of crustal stresses on fluid transport in fractured rock: case studies from northeastern and southwestern USA. Hydrogeol J 11:100–112
Morin RH, Hess AE, Paillet FL (1988) Determining the distribution of hydraulic conductivity in a fractured limestone aquifer by simultaneous injection and geophysical logging. Ground Water 26:587–595
Morin RH, Carleton GB, Poirier S (1997) Fractured-aquifer hydrogeology from geophysical logs: the Passaic formation, New Jersey. Ground Water 35:328–338
Morin RH, Senior LA, Decker ER (2000) Fractured-aquifer hydrogeology from geophysical logs: Brunswick group and Lockatong formation, Pennsylvania. Ground Water 38:182–192
Mouthereau F, Lacombe O (2006) Inversion of the Paleogene Chinese continental margin and thick-skinned deformation in the Western Foreland of Taiwan. J Struct Geol 28:1977–1993
Muldoon M, Bradbury KR (2005) Site characterization in densely fractured dolomite: comparison of methods. Ground Water 43:863–876
National Research Council (1996) Rock fractures and fluid flow: contemporary understanding and applications. National Academy Press, Washington, DC, pp 568
Niemi A, Kontio K, Kuusela-Lahtinen A, Poteri A (2000) Hydraulic characterization and upscaling of fracture networks based on multiple-scale well test data. Water Resour Res 36:3481–3497
Philip ZG, Jennings JW Jr, Olson JE, Laubach SE, Holder J (2005) Modeling coupled fracture-matrix fluid flow in geomechanically simulated fracture networks. SPE Reserv Eval Eng 8:300–309
Saar MO, Manga M (2004) Depth dependence of permeability in the Oregon Cascades inferred from hydrogeologic, thermal, seismic, and magmatic modeling constraints. J Geophys Res 109:B04204. doi:10.1029/2003JB002855
Talbot CJ, Sirat M (2001) Stress control of hydraulic conductivity in fracture-saturated Swedish bedrock. Eng Geol 61:145–153
Taylor RG, Howard KWF (1999) The influence of tectonic setting on the hydrological characteristics of deeply weathered terrains: evidence from Uganda. J Hydrol 218:44–71
Taylor RG, Howard KWF (2000) A tectono-geomorphic model of the hydrogeology of deeply weathered crystalline rock: evidence from Uganda. Hydrogeol J 8:279–294
Timur A, Toksöz MN (1985) Downhole geophysical logging. Annu Rev Earth Planet Sci 13:315–344
van der Kamp G (2001) Methods for determining the in situ hydraulic conductivity of shallow aquitards: an overview. Hydrogeol J 9:5–16
Verbovšek T (2009) Influences of aquifer properties on flow dimensions in dolomites. Ground Water 47:660–668
Walker DD, Roberts RM (2003) Flow dimensions corresponding to hydrogeologic conditions. Water Resour Res 39:1349. doi:10.1029/2002WR001511
Williams JH, Johnson CD (2004) Acoustic and optical borehole-wall imaging for fractured-rock aquifer studies. J Appl Geophys 55:151–159
Winter CL, Tartakovsky DM, Guadagnini A (2003) Moment differential equations for flow in highly heterogeneous porous media. Surv Geophys 24:81–106
Wyllie MRJ, Gregory AR, Gardner LW (1956) Elastic wave velocities in heterogeneous and porous media. Geophysics 41–70
Zhang Y, Person M, Gable CW (2007) Representative hydraulic conductivity of hydrogeologic units: insights from an experimental stratigraphy. J Hydrol 339:65–78